J. Fluid Mech. (2003), *vol.* 490, *pp.* 129–138.
DOI: 10.1017/S0022112003005408 Printed in the United Kingdom

Flow structures behind a heaving and pitching finite-span wing

By K. D. von ELLENRIEDER†, K. PARKER and J. SORIA

Laboratory for Turbulence Research in Aerospace & Combustion, Mechanical Engineering, Monash University, Clayton Campus, VIC 3800, Australia

(Received 1 October 2002 and in revised form 26 May 2003)

The three-dimensional structure of the flow behind a heaving and pitching finite-span wing is investigated using dye flow visualization at a Reynolds number of 164. Phase-locked image sequences, which are obtained from two orthogonal views, are combined to create a set of composite images that give an overall sense of the three-dimensional structure of the flow. A model of the vortex system behind the wing is constructed from the image sequences. Variations of the Strouhal number, pitch amplitude and heave/pitch phase angle are qualitatively shown to affect the structure of the wake.

1. Introduction

The forces associated with vortex shedding behind a bluff body can cause motion of the body, as in the case of aerodynamic flutter (McCroskey 1982). Conversely, a bluff body in motion within a uniform flow can impart forces to the surrounding fluid by the introduction of pressure variations and circulation at the surface of the body. For example, a circular cylinder undergoing rotary oscillations about a fixed axis of symmetry can exert a degree of control over the structure of the wake (Tokumaru & Dimotakis 1991). Similarly, when a circular cylinder is transversely oscillated in a uniform flow, the wake is affected (Bishop & Hassan 1964; Koopman 1967). At low frequencies the lift and drag forces fluctuate at multiples of the natural Strouhal frequency of the cylinder. As the oscillation frequency is increased, these forces are synchronized with the imposed oscillation frequency and the Strouhal frequency is lost. Since the lift and drag forces are caused by vortex shedding at the surface of the cylinder, the structure of the wake is strongly dependent on the driving frequency of the cylinder.

If the transversely oscillating cylinder is replaced by an airfoil, the airfoil will have a time-dependent angle of attack, which is caused by the combination of transverse motion and free-stream velocity. A normal force vector is produced, which has fluctuating thrust and lift components (Jones, Dohring & Platzer 1998). When the average thrust is lower than the drag on the airfoil, a von Kármán vortex street may be seen in the wake. On the other hand, when the average thrust force is higher than the average drag, the flow behind the airfoil has the form of a jet and the flow can exhibit a 'reverse' von Kármán vortex street (Freymuth 1988). The structure of the flow behind two-dimensional airfoils has been extensively studied (e.g. Wood & Kirmani 1970; Koochesfahani 1989; Ohmi *et al.* 1990, 1991; Anderson *et al.* 1998).

† Present address: Department of Ocean Engineering, Florida Atlantic University, Dania Beach, FL 33004-3023, USA.

In comparison, there are few studies of the flow behind finite-span wings. In this case, the interaction of the wingtip vortices with vortices shed at the leading and the trailing edges of the wing will create a flow structure which is substantially different to the two-dimensional case.

Owing to the high propulsive efficiencies measured on two-dimensional oscillating airfoils (e.g. Anderson *et al.* 1998), most investigations of three-dimensional oscillating wings have focused on directly measuring thrust production and efficiency (DeLaurier & Harris 1982; Bandyopadhyay *et al.* 2000; Ramamurti & Sandberg 2001) rather than examining the flow structure. Since the average thrust or drag produced by the airfoil is related to vortex shedding at the surface of the wing, the flow structure is important for understanding the mechanics of thrust production. Flow visualization studies by the present authors (von Ellenrieder, Parker & Soria 2001*b*, 2002; Parker, von Ellenrieder & Soria 2002, 2003) examine the separate effects of pitch angle, oscillation frequency and phase angle between pitching and heaving on the flow behind a finite span wing. Here, the overall structure of the flow is examined in greater detail for a Reynolds number of 164 (based on the airfoil chord and free-stream velocity). Bearing in mind the inherent limitations of the visualization method (see § 1.1), the main aim of this study is to gain an understanding of the large-scale structure of this complex flow.

1.1. *A note on the flow visualization method*

The flow behind a finite-span wing is unsteady and three-dimensional. Quantitative, whole-field, three-dimensional measurement techniques such as holographic particle image velocimetry HPIV (von Ellenrieder, Kostas & Soria 2001*a*) or holographic interferometry HI (Arroyo *et al.* 2001) are still in the early development stages and are difficult to implement for time-dependent flows. Other multi-component quantitative measurement techniques such as PIV and stereoscopic PIV can only provide information about the flow field one plane at a time. Using these methods, one must make extensive surveys of the flow in order to formulate a complete picture of its three dimensional structure. Without a prior knowledge of the spatial extent and nature of the flow, this approach can be extremely inefficient.

Dye flow visualization is a qualitative method but can be used to image large regions of a flow. The dye released at the surface of the oscillating wing follows the pathlines in the flow to form streaklines. The limitations of this method include (Hama 1962; Coutanceau & Defaye 1991; Lim 2000): (i) In an unsteady flow the streaklines do not necessarily coincide with the instantaneous streamlines. (ii) The dye filaments contain information, which starts at the point of introduction and is integrated along the path of the dye lines. It can be difficult to ascertain whether the shape of a streakline is the result of fluid distortion or flow memory. (iii) The Schmidt number of the dye is $O(10^3)$ – the dye will only follow the vorticity in the initial stage of flow development. (iv) The transport mechanisms for dye (a passive scalar) and vorticity are slightly different and in regions of the flow where vortices are substantially stretched, the time evolution of the dye and vorticity may not be identical.

Thus, when carrying out the experiments and interpreting the results, care is required to ensure that the streaklines give an accurate representation of the flow. The over-riding advantage of this method is that it can give an idea of the large-scale nature of the flow.

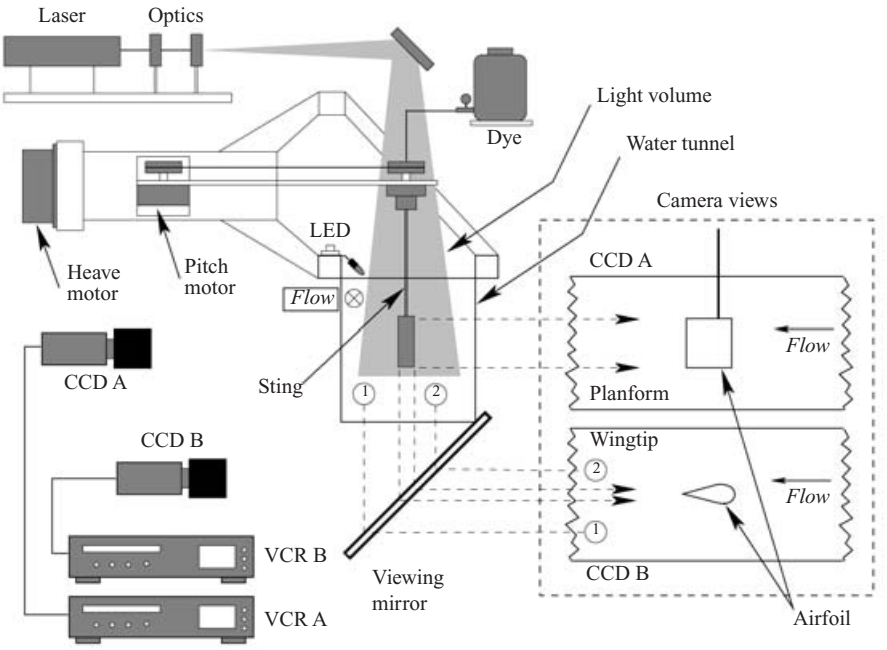

FIGURE 1. Schematic of the experimental setup. As shown by the circled numbers, objects closer to the bottom of the wingtip view are nearer to the observer in the planform view (CCD A).

2. Apparatus and technique

The experiments are performed in a re-circulating water tunnel with a 100 mm × 100 mm × 800 mm test section. The tunnel has a 9:1 area-contraction ratio between the settling chamber and the test section. The flow is driven by a centrifugal pump, and a gate valve can be used to continuously vary the average free-stream flow speed from 5 to 115 mm s^{-1}. A volumetric flow rate meter is used to determine the average velocity in the test section.

The aluminium wing has a symmetrical cross-section and rectangular planform. It is hollow, has a chord length of $c = 19$ mm, a thickness of $t/c = 0.3$ and an aspect ratio of $AR = 3.0$. A line of dye injection holes, which have a diameter of 0.9 mm, are positioned at 2.0 mm intervals along the leading edge of the wing. A brass tube (90 mm long with a 2.4 mm outer diameter) fitted into the wingtip at the quarter-chord point serves as both the sting and as part of the dye injection system.

As shown in figure 1, the foil is oscillated in pitch by using a stepper motor that drives a pulley system. A pulley mounted on the motor shaft is coupled to a second pulley mounted on the sting. This motor–sting–foil assembly is mounted on a horizontally orientated, linear translation stage. The heaving motion of the wing is produced by using a second stepper motor to actuate the translation stage. The motors are controlled using a multi-axis indexer (programmed with a desktop PC) and two high-resolution drivers (25 000 steps/mm in heave and 50 000 steps/revolution in pitch). Differential, shaft-mounted encoders with a resolution of 2048 pulses per revolution are used to obtain position feedback of the pitch and heave displacements. A cosine motion profile is used for both the heaving and pitching motion and the

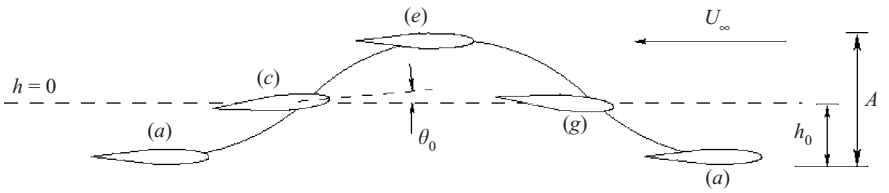

FIGURE 2. Heave and pitch motion profile for $\psi = 90°$. The solid line represents the path of the quarter-chord point and the letters (a, c, e, g, a) indicate the airfoil locations in figure 3.

Test	St	θ_0 (deg.)	ψ (deg.)
1	0.35	{0, 5, 10, 15, 20}	90
2	{0.2, 0.25, 0.3, 0.35, 0.4}	10	90
3	0.35	10	{60, 75, 90, 105, 120}

TABLE 1. Flow visualization parameters.

oscillation frequency of heave and pitch is the same. The motion is given by

$$h(t) = h_0 \cos(2\pi f t), \quad \theta(t) = \theta_0 \cos(2\pi f t + \psi), \tag{2.1a, b}$$

where $h_0 = c/2$ is the heave amplitude, θ_0 is the pitch amplitude, f is the oscillation frequency, t is time, and ψ is the phase angle between heave and pitch (figure 2). The frequency is checked by measuring the limit/home switch feedback signal from the translation stage with an oscilloscope. The double-amplitude of the quarter-chord point A is kept constant at $A/c = 1.0$, and the average free-stream velocity fixed to $U_\infty = 8.5\,\mathrm{mm\,s^{-1}}$; the Strouhal number $St = fA/U_\infty$ was then varied by changing the oscillation frequency. Note that the laboratory setup allows us to independently vary the Reynolds number $Re = U_\infty c/\nu$ (where ν is the kinematic viscosity) and Strouhal number.

The separate effects of varying θ_0, St, and ψ are investigated in a series of tests. In each case two of the parameters are fixed and the third is varied; the combinations are given in table 1. These values are in the range found to produce thrust with a high efficiency for two-dimensional oscillating foils (Anderson *et al.* 1998). The results of a preliminary examination of end effects on oscillating cylinders by Bishop & Hassan (1964) suggest that the force responses of two- and three-dimensional cylinders will be similar. Synchronization and phase shifting of the lift and drag forces on the cylinders still occurs. However, the variation of mean drag with St becomes more gradual. Hence, the values in table 1 were chosen because the dependence of both two- and three-dimensional airfoil flows on these values (especially St) is expected to be comparable.

To visualize the flow, laser light is used to illuminate fluorescent dye (Kiton Red 620), which is injected through the sting and foil from a bottle, mounted approximately 1.0 m above the test section. The dye flow rate is controlled using a small needle valve. A 200 mW Nd:YVO_4 diode laser provides the light. Two orthogonally orientated pairs of cylindrical lenses expand the laser beam into a rectangular volume of approximately $3c$ in the direction of the heaving axis and $7c$ in the streamwise direction. A viewing mirror (see figure 1) is mounted below the water tunnel to allow a planform view of the wing and a view from a second plane, which is perpendicular to the pitching axis (wingtip view), to be simultaneously recorded (see figure 3*a*, for example). The

flow visualizations are captured on VHS tape by a pair of CCD cameras with 50 mm lenses (at f/# = 1.8) and two video recorders (VCRs). The red light of the fluorescent dye is separated from the green laser light using optical filters. Fluorescent red paint is applied to the chord of the wing, and the wingtip is illuminated from below the tunnel with green light, to highlight the chordline in the images of the wingtip view. A red LED, which is in the field of view of both cameras, is briefly switched on at the beginning of each experiment to allow the two VHS tapes to be synchronized for analysis. Digitized movies of the flow are obtained from the VHS tapes using a desktop computer with an internal frame grabber. The frame-grabber software combines the digitized movies from the two viewing directions into a single composite video.

2.1. *Image analysis*

The flow visualization of each test condition, corresponding to the different pitch amplitudes, phase lead angles, and Strouhal numbers, is recorded for more than ten heave/pitch cycles. Since the frame rate of the camera is fixed at 25 frames per second (PAL video standard), and the heaving frequency for each Strouhal number is accurately known, still images can be extracted from the digitized movies at precise locations in the heave/pitch cycle. Sets of still images, at eight equally spaced time intervals during each cycle, are obtained for each test case. In the first image of each sequence the airfoil is located at the lowest extreme of the heave cycle so that the following locations are captured:

$$h/h_0 = \{-1.0,\ -0.5,\ 0,\ 0.5,\ 1.0,\ 0.5,\ 0,\ -0.5\}. \tag{2.2}$$

Thus, the still images are phase-locked to the motion of the airfoil and image sequences from each of the different test conditions are visually compared side-by-side.

3. Results and discussion

3.1. *Overall flow structure*

The evolution of the flow over one heave/pitch cycle is shown in figure 3 for $\theta_0 = 5°$, $\psi = 90°$, $St = 0.35$. Vortex structures shed from the leading edge are labelled with an L and trailing-edge vortices are denoted with a T; the subscripts correspond to different half-cycles of the motion. In the wingtip view of each image the airfoil chordline is visible as a white stripe. The side and planform views are vertically aligned to give a sense of the three-dimensional structure of the flow and the fluid is moving from right to left. The wingtip view corresponds to the view an observer would have if looking along the pitching axis of the wing. Owing to the viewing mirror setup, flow structures closest to the bottom of the wingtip view are nearer to the observer in the planform view (see figure 1).

The wingtip view of the image sequence (figure 3) shows that an L and a T vortex are shed each half-cycle when the wing is near $h/h_0 = \pm 1$. The vortices are shed in alternating order with the T vortices occurring nearer to the extrema of the heaving motion and the L vortices remaining near the mean heave ($h = 0$) position. The sequence of vortices is

$$\mathrm{T}_1 \rightarrow \mathrm{L}_1 \rightarrow \mathrm{T}_2 \rightarrow \mathrm{L}_2. \tag{3.1}$$

The planform view of each image shows that the filamentary structures formed by the T vortices are concave and those formed by the L vortices are convex relative to the downstream side of the flow (figure 3*a*, *b* for example). When the vortices

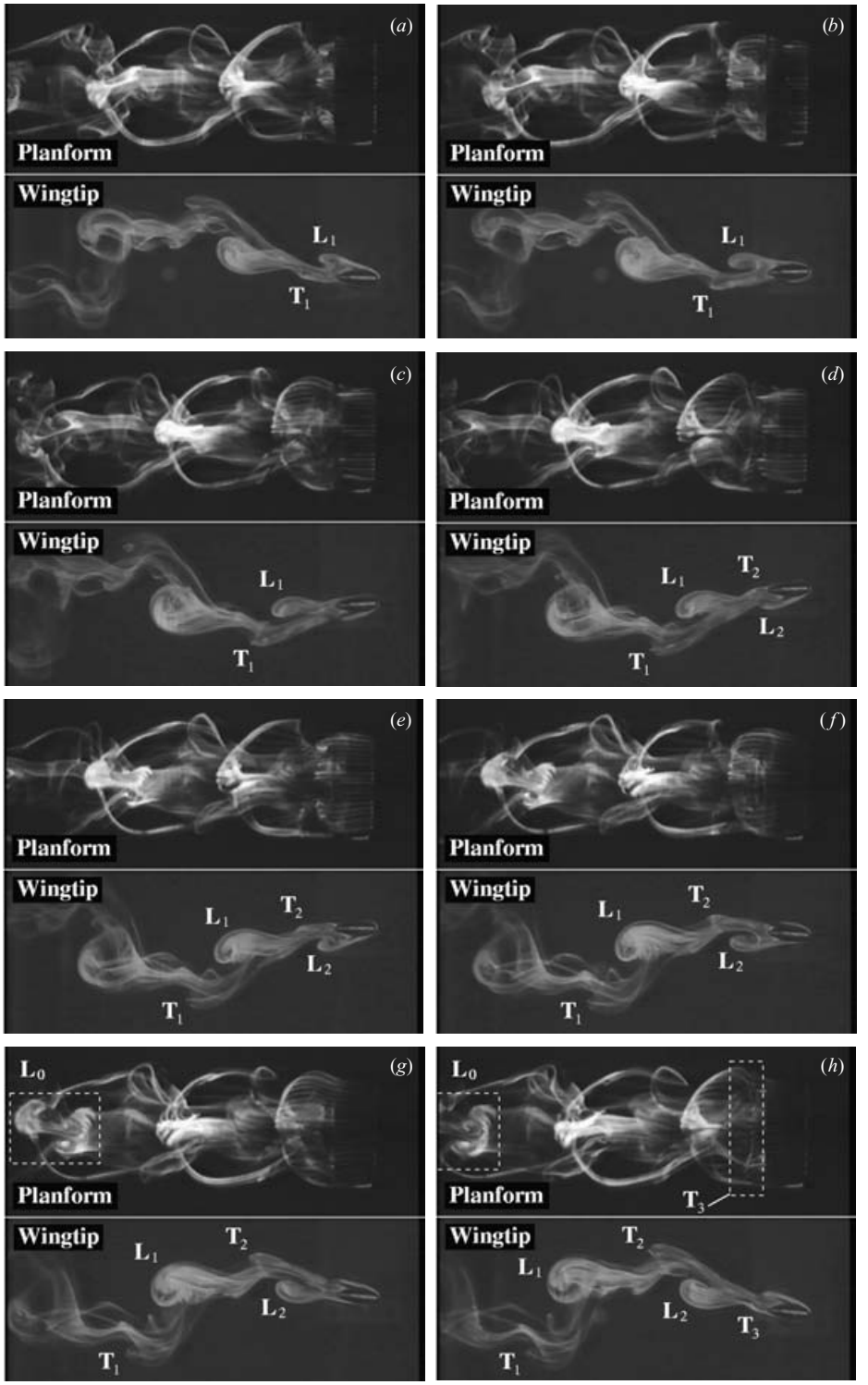

FIGURE 3. Flow sequence for $\theta_0 = 5°$; $\psi = 90°$; $St = 0.35$.

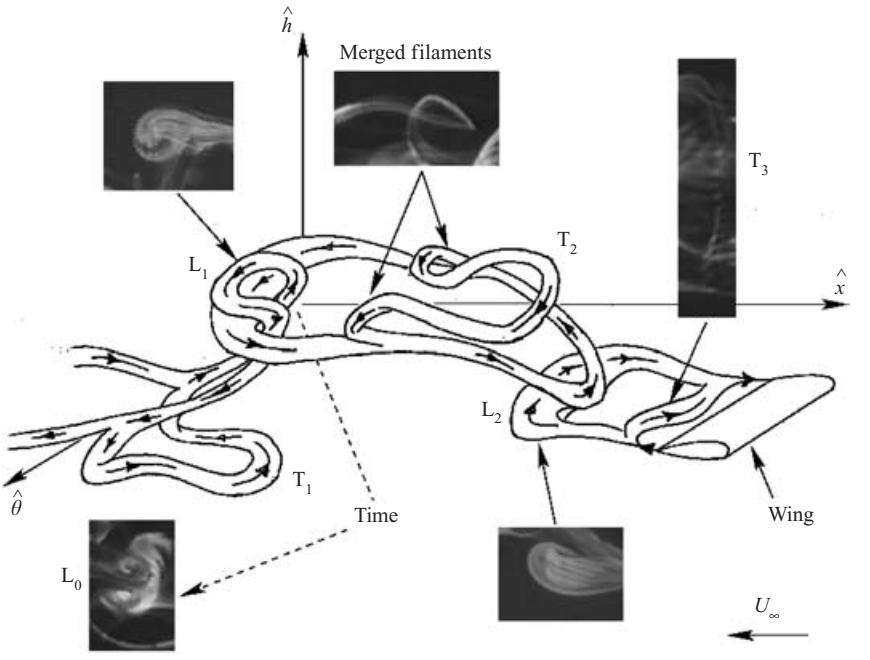

FIGURE 4. Sketch of flow structure in figure 3(*h*). See text of § 3.1 for description.

convect downstream, the L vortex is stretched. It forms a ring-like structure with a bulbous head, which lies along the midspan plane, and two filamentary arms, which extend upstream to merge with the successive T vortex (see L_1 and T_2 in the planform view of figure 3*f*). As the cycle continues, these merged filaments move toward the midspan plane and simultaneously wrap around and combine with the head of the following L vortex (figure 3*f–h*). This is dramatically apparent in the planform views of structure L_0 (figure 3*g*, *h*) where the wrapped filaments have the appearance of two oppositely directed starting vortices.

The sequence of images in figure 3 was used to construct an isometric sketch of the flow structure (figure 4), which corresponds to the part of the heave/pitch cycle in figure 3(*h*). The locations of the vortex structures in the three-dimensional sketch are found by qualitatively mapping their positions in the two orthogonal views (as shown in figure 1). Arrows lying along the vortex filaments indicate the direction of circulation as inferred from the motion of the wing and the direction of vortex roll-up. The T vortex of each half-cycle is joined to the L vortex of the preceeding half-cycle. Since these two vortices have the same direction of circulation, the arms of the T vortex must curve back upstream to connect with the L vortex, as shown by the image marked 'merged filaments' in figure 4. Some images of the other features from figure 3(*h*) are also 'overlaid' to display the correlation between the sketch and the flow visualization. L_0 is included to show that, in time, the filamentary structures wrapped around L_1 will take on a similar appearance. The planform overlay of structure T_3 is shown immediately behind the airfoil and reveals how T_3 is connected to the wingtip vortices in figure 3(*h*). T_3 is simply the T_1 vortex of the succeeding cycle and L_0 is the L_2 vortex of the previous heave/pitch cycle. In accordance with the rule that no vortex can simply begin or end in the flow, the T and L vortices form a continuous system of interconnected loops which extends upstream to the wing.

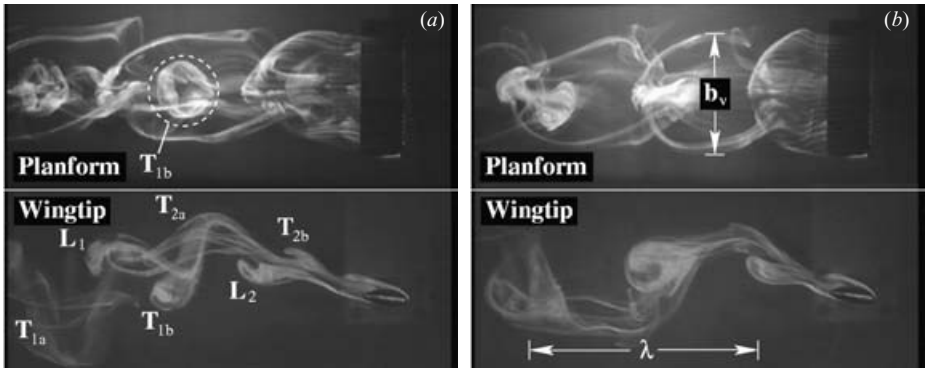

FIGURE 5. Strouhal number effects: $h/h_0 = -1$; $\theta_0 = 10^\circ$; $\psi = 90^\circ$; (*a*) $St = 0.3$, (*b*) $St = 0.4$.

Given that the flow visualization sequence in figure 3 is typical of most of the test conditions examined, the proposed structure is also expected to be common to most of the test cases.

3.2. *Pitch amplitude, St and phase angle effects*

3.2.1. *Pitch amplitude*

In all cases, the sequence of vortices shed by the airfoil is like that of the sequence in § 3.1. Generally, the order of the T and L vortices remains the same as they convect downstream, with no overtaking in the 7*c* long field of view. From the wingtip view, the flow structures have a square-wave-shaped profile at each of the different pitch amplitudes. As the pitch amplitude increases, the filamentary arms of the leading-edge vortices (see L_1 in planform view of figure 3*h*, for example) becomes less circular in shape. Additionally, the streamwise spacing of the L vortices decreases. The increased pitch rate of the wing, which occurs at the higher pitch amplitudes, may cause the L vortices to shed at earlier parts of the heave/pitch cycle.

3.2.2. *St*

When $St = 0.2$ the wake has the saw-tooth wave appearance of a wake instability super-imposed on the cosine-shaped path of the wing. At $St = 0.25$ the airfoil motion produces the usual vortex sequence of § 3.1. At $St = 0.3$ the sequence changes and two T vortices and one L vortex are shed each half-cycle in the order: $T_{1a} \rightarrow L_1 \rightarrow T_{1b} \rightarrow T_{2a} \rightarrow L_2 \rightarrow T_{2b}$. The extra T_b vortex per half-cycle is manifested by the formation of ring-like structures inside the filamentary arms of the L vortices (figure 5*a*). When $St = 0.35$ and 0.4 the wake sequence returns to that of (3.1). Generally, as the Strouhal number is increased the spanwise size of the vortex structures b_v also increases, whereas the streamwise wavelength λ of the wake decreases (figure 5*b*).

3.2.3. *Phase angle*

The variation of ψ seems to most strongly affect the timing of the shedding of the leading- and trailing-edge vortices. At $\psi = 60^\circ$, T_1 slowly sheds from the wing, allowing L_1 to overtake it while the shedding process is still occurring. The resulting flow sequence is: $L_1 \rightarrow T_1 \rightarrow T_2 \rightarrow L_2$. In the planform view of figure 6 it can be seen that the L_1 and T_2 filaments merge as shown in figure 4, but instead of the merged filaments simply being wrapped around the following L_2 structure, the anomalous

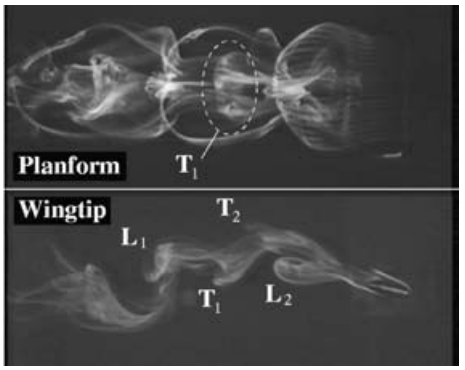

FIGURE 6. $h/h_0 = -1$; $\theta_0 = 10°$; $\psi = 60°$; $St = 0.35$.

T_1 structure appears in the middle of every other loop. As ψ increases the sequence progressively becomes more like that of § 3.1.

4. Concluding remarks

The variation of θ_0, St and ψ has observable effects on the structure of the wake. However, the flow visualization sequence of figure 3 is representative of the most commonly seen flow patterns in the present experiments and suggests the three dimensional model of the vortex structure proposed in figure 4. As discussed in § 2, the selection of the test parameters (table 1) is based on the hypothesis that the force responses of two- and three-dimensional wings will have a similar dependence on St. However, the verification of this possibility, as well as a physical explanation for the dynamical significance of the many observed flow structures, requires quantitative measurements.

REFERENCES

ANDERSON, J. M., STREITLIEN, K., BARRETT, D. S. & TRIANTAFYLLOU, M. S. 1998 Oscillating foils of high propulsive efficiency. *J. Fluid Mech.* **360**, 41–72.

ARROYO, M. P., VON ELLENRIEDER, K. D., LOBERA, J. & SORIA, J. 2001 Measuring 3-C velocity fields in a 3-D flow domain with HPIV and HI. In *Proc. 4th Intl Workshop on Particle Image Velocimetry* (ed. J. Kompenhans). DLR e.V.

BANDYOPADHYAY, P. R., CASTANO, J. M., NEDDERMAN, W. H. & DONNELLY, M. J. 2000 Experimental simulation of fish-inspired unsteady vortex dynamics on a rigid cylinder. *Trans. ASME: J. Fluids Engng* **122**, 219–238.

BISHOP, R. E. D. & HASSAN, A. Y. 1964 The lift and drag forces on a circular cylinder oscillating in a flowing fluid. *Proc. R. Soc. Lond.* A **277**, 51–75.

COUTANCEAU, M. & DEFAYE, J. R. 1991 Circular cylinder wake configurations: A flow visualization survey. *Appl. Mech. Rev.* **44**, 255–305.

DELAURIER, J. D. & HARRIS, J. M. 1982 Experimental study of oscillating-wing propulsion. *J. Aircraft* **19**, 368–373.

VON ELLENRIEDER, K. D., KOSTAS, J. & SORIA, J. 2001*a* Measurements of a wall-bounded, turbulent, separated flow using HPIV. *J. Turbulence* **2**, 004.

VON ELLENRIEDER, K. D., PARKER, K. & SORIA, J. 2001*b* Visualization of a three dimensional heaving aerofoil foil. In *Proc. 14th Australasian Fluid Mech. Conf* (ed. B. B. Dally), pp. 151–154. Casual Productions Pty. Ltd.

VON ELLENRIEDER, K. D., PARKER, K. & SORIA, J. 2002 Visualization of the three dimensional flow behind oscillating foils. *AIAA Paper* 2002-0696.

Freymuth, P. 1988 Propulsive vortical signature of plunging and pitching airfoils. *AIAA J.* **26**, 881–883.

Hama, F. R. 1962 Streaklines in a perturbed shear flow. *Phys. Fluids* **5**, 644–650.

Jones, K. D., Dohring, C. M. & Platzer, M. F. 1998 Experimental and computational investigation of the Knoller-Betz Effect. *AIAA J.* **36**, 1240–1246.

Koochesfahani, M. M. 1989 Vortical patterns in the wake of an oscillating airfoil. *AIAA J.* **27**, 1200–1205.

Koopman, G. H. 1967 The vortex wakes of vibrating cylinders at low Reynolds numbers. *J. Fluid Mech.* **28**, 501–512.

Lim, T. T. 2000 Dye and smoke visualization. In *Flow Visualization: Techniques and Examples* (ed. A. J. Smits & T. T. Lim), chap. 3, pp. 43–72. Imperial College Press.

McCroskey, W. J. 1982 Unsteady airfoils. *Annu. Rev. Fluid Mech.* **14**, 285–311.

Ohmi, K., Coutanceau, M., Daube, O. & Loc, T. P. 1990 Vortex formation around an oscillating and translating airfoil at large incidences. *J. Fluid Mech.* **211**, 37–60.

Ohmi, K., Coutanceau, M., Loc, T. P. & Dulieu, A. 1991 Further experiments on vortex formation around an oscillating and translating foil at large incidences. *J. Fluid Mech.* **225**, 607–630.

Parker, K., von Ellenrieder, K. D. & Soria, J. 2002 The effects of phase angle on the vortical signatures behind a flapping airfoil of finite aspect ratio. In *Proc. 10th Intl Symp. on Flow Visualization* (ed. T. Kobayashi & M. Kawahashi), Paper F0368. Visualization Society of Japan.

Parker, K., von Ellenrieder, K. D. & Soria, J. 2003 Flow visualization of the effect of pitch amplitude changes on the vortical signatures behind a three dimensional flapping airfoil. In *Optical Technology and Image Processing for Fluids and Solids Diagnostics* (ed. G. X. Shen, S. S. Cha, F. P. Chiang & C. R. Mercer). *Proc. SPIE*, vol. 5058, pp. 331–343.

Ramamurti, R. & Sandberg, W. C. 2001 Computational study of 3-d flapping foil flows. *AIAA Paper* 2001-0605.

Tokumaru, P. T. & Dimotakis, P. E. 1991 Rotary oscillation control of a cylinder wake. *J. Fluid Mech.* **224**, 77–90.

Wood, C. J. & Kirmani, S. F. A. 1970 Visualization of heaving airfoil wakes including the effect of a jet flap. *J. Fluid Mech.* **41**, 627–640.